Defining the Impact of Cell-Type and Species on the Molecular RNA Replication Kinetics of Seoul Virus

Autumn T. LaPointe[a], Stefan D. Klimaj[a], and Alison M. Kell[a#]

[a]Department of Molecular Genetics and Microbiology, University of New Mexico School of Medicine, Albuquerque, New Mexico, United States of America

[#]Address correspondence to Alison M. Kell, amkell@salud.unm.edu

Keywords

Seoul Virus; RNA Replication; qRT-PCR; Negative-stranded segmented virus

Abstract

Hantaviruses are zoonotic, tri-segmented, negative-sense RNA viruses and a significant public health threat. Viral pathogenesis varies between host species, with rodent reservoir infection being asymptomatic and human infection resulting in severe, immune-mediated disease. Viral pathogenesis is highly dependent on virus replication efficiency since it affects the virus's ability to evade detection and determines the magnitude of the host immune response. However, the molecular replication kinetics for hantaviruses remain poorly defined. Therefore, we developed a sense- and segment-specific quantitative real-time PCR (ssqRT-PCR) assay and a SYBR-based qRT-PCR (Sb-qRT-PCR) assay, allowing us to quantify both negative-sense genome levels and

total viral RNA synthesis of the small (S), medium (M), and large (L) segments of Seoul virus (SEOV). We then measured total viral RNA and genome accumulation in reservoir rat endothelial cells (RLMVEC), non-reservoir human endothelial cells (HUVEC-C), and Vero E6 epithelial cells. We also measured the ratio of each segment released into the culture supernatant, approximating the relative packaging efficiency. We found that, while the magnitude of viral RNA differed, RNA replication kinetics were largely similar between reservoir and non-reservoir endothelial cells. However, replication and release kinetics differed between infection of endothelial and Vero cells. We also found that the S, M, and L segments were not equally abundant during viral infection or release, but instead followed a trend of M>L>S. Overall, this study validates two qRT-PCR assays to measure SEOV RNA, details the accumulation and release of each viral segment, and demonstrates the impact of host cell type on hantavirus replication.

Impact Statement

Hantavirus infections in humans lead to significant immune-mediated morbidity and mortality around the world and pose a threat to public health. Zoonotic transmission occurs from persistently infected rodents which show no overt signs of disease. Understanding the molecular interactions that drive divergent infection outcomes is incomplete in the field of hantavirus research due to limited tools and reagents. This novel strand- and segment-specific quantitative RT-PCR assay uncovers the unique kinetics of hantavirus genome replication in reservoir and non-reservoir cells. Further, this assay will serve as a valuable tool to investigate antiviral therapies and virus-host interactions critical for polymerase activity.

48 ## Introduction

49 Hantaviruses are negative-sense, segmented RNA viruses which are maintained
50 worldwide in rodent and insectivore reservoirs [1, 2]. While infection of the rodent
51 reservoir is typically asymptomatic and persistent, hantavirus infection of humans can
52 result in severe disease [3]. In the case of Old World hantaviruses, disease manifests
53 as hemorrhagic fever with renal syndrome (HFRS) with a mortality rate of up to 12% [4,
54 5]. Meanwhile, infection with New World hantaviruses results in hantavirus
55 cardiopulmonary syndrome (HCPS) with a mortality rate of up to 60% [6, 7].

56 Hantavirus infection in both the rodent reservoir and human host primarily targets
57 endothelial cells [8, 9]. Infection of human endothelial cells leads to immune activation in
58 cell culture, which may contribute to overall immune-mediated disease [7, 10, 11]. For
59 Old World hantaviruses, the RNA recognition receptors retinoic acid-inducible gene I
60 (RIG-I) and melanoma differentiation-associated protein 5 (MDA5) are required for type
61 I interferon (IFN) signaling [7, 11, 12]. The RNA pathogen-associated molecular pattern
62 (PAMP) that is detected by RIG-I during hantavirus infection remains unknown.
63 Hantavirus infection of the rodent reservoir is asymptomatic *in vivo* and fails to drive
64 significant type I IFN signaling after viral entry *in vitro* [1, 2, 13-15]. This lack of immune
65 response is not due to direct antagonism of RIG-I by viral proteins [7]. It is therefore
66 possible that the differences seen in immune response to SEOV infection between
67 human and rat endothelial cells may be due to differential production of viral RNA
68 PAMPs that could be detected by RIG-I. Alternatively, infection by incomplete viral
69 particles that contain only one or two segments instead of three could also lead to
70 immune sensing of improperly hidden PAMPs resulting in an inflammatory immune

71 response. However, current knowledge of the RNA replication kinetics and genome
72 release of SEOV in endothelial cells remains limited.

73 The SEOV genome is composed of three negative-sense RNA segments termed
74 small (S), medium (M), and large (L) based on their respective sizes. During viral
75 infection, two positive-sense RNA species are produced for each segment: the
76 antigenome, which serves as template for genome replication, and the viral mRNA [16-
77 18]. Since the genomic RNA is packaged into viral particles, it represents the product of
78 viral replication. As such, genome abundance represents the sum of viral replication
79 and particle release. However, since we currently do not know which viral RNA species
80 (i.e. positive-sense or negative-sense) leads to the activation of the immune response,
81 understanding viral RNA synthesis as a whole is also important.

82 In order to measure the RNA replication kinetics of SEOV, we developed a
83 TaqMan strand-specific, quantitative, reverse-transcription, real-time PCR assay
84 (ssqRT-PCR) to quantify viral genome abundance specifically as well as a SYBR-based
85 quantitative, real-time PCR (Sb-qRT-PCR) assay to measure total viral RNA synthesis
86 for each segment. Using these assays, we measured SEOV RNA accumulation and
87 release over time in cell cultures. Rat and human endothelial cells represent the target
88 cells for SEOV infection the reservoir and non-reservoir host, respectively. Additionally,
89 we quantified SEOV RNA kinetics in Vero E6 cells, as they are an ubiquitous epithelial
90 cell line used for hantavirus propagation and allowed us to measure SEOV replication in
91 the absence of type I IFN. We hypothesized that there would be significant differences
92 in RNA replication kinetics between the human and reservoir rat endothelial cells, but
93 that RNA replication would be similar between the rat endothelial cells and Vero E6

94 cells, as neither mount a significant type I IFN response to SEOV infection. However,
95 we instead observed viral replication in both human and rat endothelial cells to have
96 similar kinetics to each other, yet unique compared to infected Vero E6 epithelial cells.
97 Similar to previous reports, overall RNA abundance in reservoir endothelial cells was
98 higher than in human endothelial cells, suggesting a general infection advantage. We
99 also noted differential abundance of the S, M, and L segments, following a consistent
100 pattern of M > L > S across all three cell species. Collectively, this study presents a
101 strand-specific qRT-PCR assay used to quantify SEOV RNA replication in reservoir and
102 non-reservoir host species and suggests that cell type may impact viral replication
103 kinetics.
104

105 ## Results

106 **qRT-PCR assay design**

107 To target the negative-sense genome for cDNA synthesis, we designed cDNA
108 primers complementary to the genome for each segment. These primers included a
109 unique tag sequence on the 5' end to prevent self-priming (Fig 1A) [19, 20]. Real-time
110 PCR primers targeting the unique tag sequence (3') and viral genome (5') were used to
111 amplify the cDNA and TaqMan probes specific for each segment were used for
112 detection.

113 As a corollary to the ssqRT-PCR, we also designed segment-specific primers for
114 a SYBR green assay (Sb-qRT-PCR) to measure total viral RNA (genome, antigenome,
115 and viral mRNA) for each segment. Random primers were used for cDNA synthesis so

116 that both the negative and positive sense RNAs are intentionally primed. Segment-
117 specific primers were then used for the subsequent qRT-PCR step (Fig. 1A).
118
119 **qRT-PCR assay validations**
120 To validate our assays, we *in vitro* transcribed (IVT) negative-sense RNAs for
121 each SEOV segment from PCR templates. While we were able to transcribe the full-
122 length S genome, we were unable to obtain full length M and L genomes, so 500nt
123 segments spanning the primer and probe binding regions were used for the M and L
124 genomes instead. These IVT RNAs were used as template for first-strand cDNA
125 synthesis. Utilizing first-strand reverse transcription minimizes any bias in efficiency due
126 to differences in template length, as these efficiency differences are not repeatedly
127 perpetuated in a single cycle reaction as they would be in a typical, multi-cycle PCR
128 reaction. The cDNA was then serially diluted to make a standard curve from 10^6-10^0
129 copies of input RNA for qRT-PCR. To confirm that the ssqRT-PCR assay detected only
130 specifically primed RNA and not self-primed RNA, we included a negative control cDNA
131 synthesis reaction without cDNA primers. For the S, M, and L negative-sense IVT
132 RNAs, the ssqRT-PCR assay reliably detected down to 10^3 molecules of input RNA,
133 and when a line of best fit was applied, all three segments had R^2 values of 0.99
134 indicating linear changes across the standard curve (Fig. 1B).
135 To test the segment specificity, IVT negative-sense RNAs of either S, M, or L
136 were used as template for each segment's assay (cDNA primer, qRT primers, and
137 probe). For example, the S segment IVT RNA was used as template for the M assay
138 primer/probe set as well as for the L assay primer/probe set (Fig 1C). For all three

139 segments in the ssqRT-PCR assay, amplification was only detected when template
140 RNA and primer/probe sequences were matched, demonstrating that the assays are
141 segment specific (Fig 1C).

142 To validate the sense specificity of the ssqRT-PCR assay, either genomic or
143 antigenomic IVT RNA for each segment was used as template for cDNA synthesis. For
144 the S and L genomic primers and probes, antigenomic RNA was only detected when
145 10^6 copies were added to the reaction, giving C_t values of 38 and 34 respectively (Fig.
146 1D). This correlates with an 11 C_t value difference in detection between the genomic
147 and antigenomic RNAs for the S segment and a 7 C_t value difference in detection for
148 the L segment. To address the potential contribution of antigenomic RNA to detection,
149 C_t cutoffs were set at C_t 38 for S and C_t 34 for L, so that values falling at or below these
150 limits would be considered background detection for future experiments. Unlike S and L,
151 M antigenomic RNA could be detected down to 10^4 copies with the primers intended to
152 detect only genomic RNA and only illustrated a 4.5 C_t value difference in detection
153 between the genomic and antigenomic RNAs (Fig 1D). Detection of the antigenomic M
154 RNA remained consistent despite testing multiple different cDNA and qRT primers and
155 PCR conditions (data not shown). Limiting detection for the M segment based on
156 antigenome detection severely reduced the range of detection for the genome.
157 Therefore, the primers and probe used for the M segment are not considered to be
158 sense-specific. This validation test was only conducted for the ssqRT-PCR, where
159 specificity for the negative sense RNA was critical to the assay's function, and not for
160 the Sb-qRT-PCR assay, where both positive and negative sense RNA will be amplified
161 and detected simultaneously.

162 For the Sb-qRT-PCR assay, the S segment was sensitive to 10^1 molecules of
163 input RNA, while the M and L segments were sensitive to 10^3 molecules RNA (Fig. 1E).
164 When a line of best fit was applied to the standard curves, all segments had R^2 values
165 of 0.99. Sb-qRT-PCR segment specificity was tested the same as the ssqRT-PCR
166 assay, where IVT negative-sense RNAs of either S, M, or L were used as template for
167 each segment's assay (cDNA primer and qRT primers). For the Sb-qRT-PCR assay for
168 S and L, non-target segments (M and L for S assay, S and M for the L assay) were
169 detected at C_t values of 39 or greater, at or near the limit of detection of the assay (C_t
170 40) (Fig 1F). In addition to this, the gap in detection between the intended segment and
171 the non-target segments was approximately 9-10C_t (equivalent to ~3 log). Given that
172 the non-target segments were measured close to the limit of detection of the assay and
173 the large difference in C_t between the target and non-target segments, it was
174 determined that detection of non-target segments was unlikely to significantly contribute
175 to the measurement of the intended segment for S and L. The Sb-qRT-PCR assay for M
176 detected non-target S and L segments at C_t values of ~36 when 10^6 copies were
177 added. To address the potential contribution of S and L RNA to detection of M, a limit of
178 detection was set at C_t 36 for M, so that values falling at or below this limit would be
179 considered background detection.
180 In order to compare SEOV replication kinetics during infection of reservoir and
181 non-reservoir species, it was important to validate that the primers and probes designed
182 for the ssqRT-PCR and Sb-qRT-PCR assays did not detect cellular RNAs from either
183 the rodent reservoir or human cells. To test this, 500ng cellular RNA isolated from
184 uninfected human umbilical vascular endothelial cells (HUVEC-C) or primary rat lung

185 microvascular endothelial cells (RLMVEC) was used as template for cDNA synthesis
186 followed by either ssqRT-PCR or Sb-qRT-PCR (Supp. Fig. 1A and 1B). None of the
187 ssqRT-PCR assays detected host RNAs from either HUVEC or RLMVEC (Supp. Fig.
188 1A) For the M segment SB-qRT-PCR, host RNAs were detected at 39 C_t, but these
189 were greater than the previously set C_t cutoff and would be treated as background in
190 future experiments (Supp. Fig. 1B).
191 We further demonstrate that the addition of non-target RNAs did not interfere
192 with the detection of the intended viral RNAs. To do this, 150ng of either HUVEC or
193 RLMVEC RNA was mixed with 10^6 copies of each of the genomic and antigenomic S,
194 M, and L IVT RNAs. This mixture was then used as template for either the ssqRT-PCR
195 or Sb-qRT-PCR assay and was compared to a standard curve for the target genome or
196 segment. For both the ssqRT-PCR assay (Fig. 2A and 2B) and Sb-qRT-PCR (Fig. 2C
197 and 2D), the dilution series made by the host/virus RNA mixture closely mirrored the
198 standard curves made using a single genomic IVT RNA for all three segments,
199 indicating that the non-target cellular or viral RNAs do not interfere with target RNA
200 detection for either assay.
201
202 **Quantification of viral RNA in SEOV infection**
203 To measure SEOV RNA replication kinetics, HUVEC, RLMVEC, and Vero E6
204 cells were infected with a cell-specific multiplicity of infection (MOI) of 0.1 focus-forming
205 units (FFU)/cell. Cell-specific MOI was determined as previously described to ensure
206 that each cell type received the infectious units required for 10% infection of the culture
207 [7]. This was done to account for differences in cell susceptibility to infection, allowing

208 us to study RNA accumulation from a more equivalent baseline of infection. Cells were
209 harvested every 24hrs over three days to capture viral RNA accumulation. Because the
210 ssqRT-PCR assay to detect M genome was not sense-specific, only the S and L
211 genomes were quantified in SEOV-infected cells. Viral replication in HUVEC displayed a
212 ~3.7 fold increase in S genomic RNA from 0dpi to 1dpi and a ~6.7 fold increase in S
213 genomic RNA, while the L genomic RNA increased ~1.7 fold from 0dpi to 1dpi and
214 increased ~2.8 fold from 1dpi to 2dpi (Fig. 3A, Supp. Table 1). After 2dpi, both S and L
215 genomic abundance in HUVEC plateaued. S and L genomic RNA levels in infected
216 RLMVEC increased ~101 fold for S and ~65 fold for L from 0dpi to 1dpi, but then
217 remained largely the same for the remainder of the infection. Conversely, infection of
218 Vero cells resulted in increases in S and L genomic RNA across all three days. The S
219 genome levels in infected Vero cells increased ~9 fold from 0dpi to 1dpi, ~5 fold from
220 1dpi to 2dpi, and ~3.5 fold from 2dpi to 3dpi. Meanwhile L genome levels increased ~5
221 fold from 0dpi to 1dpi, ~6 fold from 1dpi to 2dpi, and ~3.5 fold from 2dpi to 3dpi.
222 Cumulatively, from 1dpi to 3dpi, the S genome levels increased ~16.4 fold and L
223 genome increased ~22.4 fold in infected Vero cells.
224 The ratio of L genome to S genome produced was also calculated for each cell
225 type over the course of infection. For all three cell cultures, the L genome was found to
226 be more abundant than the S genome at all timepoints. In general, the significantly
227 higher ratio of L : S produced during infection of RLMVEC means a greater abundance
228 of L genome was produced relative to S genome compared to the HUVEC or Vero cells
229 (Fig. 3B, Supp. Table 2). Additionally, the ratio of L : S in RLMVEC increased over the

230 course of infection, while the ratio of L : S remained more equivalent across the three
231 days for infected HUVEC and Vero cells.
232 We also used the Sb-qRT-PCR assay to measure the combined accumulation of
233 the genome, antigenome, and mRNA for each segment. This allowed us to quantify viral
234 RNA synthesis as a whole as opposed to viral replication of the genome alone. Again,
235 we observed that, after an initial increase in abundance between 0dpi and 1dpi, the
236 abundance for all three segments remained steady in HUVEC and RLMVEC (Fig. 3C,
237 Supp. Table 3). S, M, and L RNA levels increased ~12 fold, ~6.3 fold, and ~3.4 fold form
238 respectively in infected HUVEC, but then only increased ~2.4 fold, ~1.7 fold, and ~4.6
239 fold respectively between 1dpi and 3dpi in infected HUVEC. Meanwhile in infected
240 RLMVEC, S, M, and L RNA levels increased ~117 fold, ~61.6 fold, and ~58.6 fold
241 respectively from 0dpi to 1dpi, but then increased only ~2.1 fold, ~3 fold, and ~3.1 fold
242 respectively from 1dpi to 3dpi. Consistent increases in abundance for all three
243 segments were observed during Vero cell infection. S, M and L RNA levels increased
244 ~19.6, ~11.7, and ~8.8 fold respectively from 0dpi to 1dpi. All three segments increased
245 ~5 fold from 1dpi to 2dpi and both M and L RNA levels increased ~10 fold from 2dpi to
246 3dpi, while S RNA levels increased ~7.5 fold from 2dpi to 3dpi. Cumulatively, from 1dpi
247 to 3dpi RNA levels increased ~40 fold, ~50 fold, and ~56 fold for S, M, and L
248 respectively in the infected Veros. The M segment was the most abundant in all three
249 host species, followed by L segment and then the S segment. Calculating the ratio of M
250 : S for each cell culture found largely similar relative abundances (Fig. 3D, Supp. Table
251 4). Likewise, the ratio of L : S and M : L were also remarkably similar between cell
252 cultures and over the course of infection. Although some of these ratios were found to

253 be statistically significantly different between cell types, the magnitude of the difference
254 is modest. Overall, while the RNA accumulation for each segment suggests that SEOV
255 RNA replication may differ between these cells, the ratios between segments remain
256 largely unchanged over the course of infection and between cell types.

257 To determine whether the trends observed in genomic and total SEOV RNA
258 synthesis were also observed in particle production, supernatants from the above
259 infected cells were collected. A focus-forming unit (FFU) assay was used to determine
260 viral titer while the ssqRT-PCR assay was used to measure genome release. Trends in
261 viral titer largely follow what was observed for viral RNA replication, with titers from the
262 human and rat endothelial cells increasing 2.5 and 4.5 fold respectively from 1dpi to
263 2dpi and then plateauing (Fig. 4A). Titer from Vero cells increased ~10.6 fold from 1dpi
264 to 2dpi and then ~2.3 fold from 2dpi to 3dpi. To measure genome copies released from
265 infected cells, viral particles were purified by ultracentrifugation through a 30% sucrose
266 cushion to remove cell debris and naked RNA that might influence the ssqRT-PCR
267 assay. Although the ssqRT-PCR was not used for measuring intracellular M genome in
268 Figure 3, this assay was used to measure the amount of M genome being released, as
269 the negative-sense genome is the dominant RNA species in bunyavirus particles [21].
270 Importantly, this assay does not determine which segments are packaged together in a
271 single virion, but simply the rate at which each segment is released in particles from the
272 cell. The quantified abundance of each segment released largely reflected our
273 intracellular observations, with M being the most abundant, followed by L, then S (Fig.
274 4B). S segment abundance increased during infection of HUVEC between days 1 and
275 2 post infection ~25 fold and then plateaued, while M segment release remained

276 equivalent between 1dpi and 2dpi and then increased ~6.5 fold form 2dpi to 3dpi (Supp.
277 Table 5). L segment abundance remained steady across all three days. For infected
278 RLMVEC, S segment abundance increased ~10 fold from 1dpi to 2dpi, then decreased
279 ~2.5 fold from 2dpi to 3dpi. Meanwhile the M segment remained steady over all three
280 days and the L segment only increased ~2.8 fold between 1dpi to 2dpi. S genome
281 release from infected Vero cells increased consistently across all three days, ~4 fold
282 from 1dpi to 2dpi and ~6.3 fold from 2dpi to 3dpi. M genome release increased ~2.6 fold
283 from 2dpi to 3dpi and L genome increased ~2.8 fold from 1dpi to 2dpi then remained
284 steady. Calculating the ratio of each segment released, the ratio of M : L segment
285 released from HUVEC was significantly smaller compared to the ratio of M : L released
286 from RLMVEC and Vero cells on days 1 and 2 post infection (Fig. 4C, Supp. Table 6).
287 Infected HUVEC also released a significantly larger ratio of L : S. Meanwhile, the ratios
288 of M : S, L : S, and M : L released from infected RLMVEC and Vero cells are similar
289 between the two cell types, with the exception of M : L at 3dpi where the ratio was
290 significantly smaller for RLMVEC infection compared to Vero.
291

292 ## Discussion

293 The strand-specific qRT-PCR assay can specifically measure the negative sense
294 genome segments of SEOV, and represents the first system to do so for a hantavirus.
295 To complement this assay and obtain a holistic view of SEOV replication, we also
296 designed a SYBR based qRT-PCR assay that measures the total viral RNA produced
297 for each segment. The ssqRT-PCR and Sb-qRT-PCR assays allowed us to conduct an
298 analysis of SEOV RNA replication and release in multiple cell types. This work builds on

299 previous studies in the hantavirus field which used qRT-PCR to characterize the
300 production of viral mRNA in Sin Nombre virus (SNV) and total viral RNA synthesis and
301 release in Puumala virus (PUUV) [18, 22]. While our study of SEOV total RNA
302 replication indicated that M segment was the most abundant in cells, followed by L and
303 then S, SNV and PUUV were reported to produce the S segment most abundantly,
304 followed by M and then L. The MOI used in these studies could be a technical
305 explanation for this discrepancy. The previous studies used an MOI of 6 or 10 infectious
306 units per cell in order to quantify viral RNA replication within the first hours of infection.
307 Conversely, we conducted infections at an MOI of 0.1 FFU/cell to limit the potential
308 impact of defective interfering particles. Using a higher MOI, while potentially necessary
309 to measure RNA replication at early timepoints, could lead to multiple simultaneous
310 entry events and replication of defective genomes [23-25]. This could result in increased
311 abundance of a particular segment that would not occur if only one infectious unit
312 entered a cell. An additional biological explanation for the differences we see in
313 segment abundances is that SNV and PUUV genomes encode an additional
314 nonstructural protein on their S segment, termed NSs, not found in SEOV [26, 27].
315 While NSs expression or putative sequences have been observed for hantaviruses with
316 rodent reservoirs in the Cricetidae family (e.g. SNV, Andes virus, and PUUV),
317 hantaviruses that infect rodents from the Muridae family (e.g. SEOV and Hantaan virus)
318 lack an NSs [28, 29]. Since both SNV and PUUV encode both the NSs and N on the S
319 segment, it is possible that hantaviruses with an NSs might produce more S segment
320 than those which only encode one protein on the S segment. A more extensive study
321 measuring the RNA replication of multiple hantaviruses at different MOIs and times post

322 infection is necessary to clarify the relative differences seen in segment abundance
323 between these studies. Interestingly, a recent study involving distantly related
324 phleboviruses, found the M genome untranslated regions (UTR) of Heartland virus to be
325 the most efficient for transcription and replication, followed by the L UTR and then the S
326 UTR [30]. Future work applying the SEOV minigenome system could determine whether
327 this is also true for hantaviruses and might explain our findings here [31]. Furthermore,
328 while the current study focused on utilizing the ssqRT-PCR and Sb-qRT-PCR assays to
329 measure SEOV, they have not been validated as specific for SEOV compared to other
330 hantaviruses and therefore should not be used in a diagnostic setting. Determining the
331 viral specificity of these assays remains an avenue for future work.
332 Notably, using the SYBR assay, the ratio of total RNA species quantified
333 between segments remained fairly similar over the course of infection, especially the
334 ratio of L : S. This suggests that total RNA of each segment is produced at similar rates.
335 The fact that the ratios of the total RNA produced for each segment are largely
336 consistent during infection means that the differences seen in RNA copy abundance
337 between segments are not due to the rates at which each segment is produced, but
338 instead are likely due to early infection events. One potential explanation could be
339 unequal packaging of S, M, and L genomes into particles in the viral stocks, which could
340 lead to differences in RNA abundance after viral entry. However, for this to be the sole
341 cause for the differences in abundance between each segment, there would need to be
342 an almost two log difference between incoming genome segments. Therefore, unequal
343 packaging of genomic segments in the viral stock particles is unlikely to be the sole
344 contributing factor. Alternatively, it is also possible that replication of the S, M, and L

345 segments is initiated at different times, leading to the difference seen in RNA
346 abundance. This idea that replication of each segment may start at different times is
347 supported by Hutchinson et al, who observed that amplification of the S mRNA was the
348 first to be detected at 4hpi, followed by M mRNA at 8hpi, and then L mRNA at 48hpi in
349 SNV infection [18]. Minor differences in segment ratios for total viral RNA synthesis over
350 the course of infection of all three cell types suggests a conserved mechanism for
351 regulating viral RNA production. Therefore, targeting these conserved mechanisms
352 used for RNA replication or the pathways that dictate when replication of each segment
353 is initiated may be useful strategies for antiviral development.

354 Similar to what has been observed for PUUV, general trends in genome release
355 reflect total intracellular viral RNA [22]. We observed that in both genome release and
356 intracellular RNA synthesis M is the most abundant followed by L and S. We also
357 observed similar kinetic trends, with infected HUVEC and RLMVEC showing slight
358 increases in genome release, but consistently larger increases in genome release as
359 Vero infection progressed. However, one interesting difference observed was that the
360 abundance of M and L genomes that were released from infected HUVEC are very
361 similar compared to infection of the other two cell types, where M and L genome
362 abundance differ by a log or more. Future studies will be needed to determine if these
363 differences in SEOV genome release are solely immune-mediated or result from
364 differences in host : virus interactions.

365 While it was unexpected to find that the segments were released in different
366 ratios, it is important to note that the qRT-PCR assays used do not determine co-
367 packaging or whether the RNA is replication competent, but only the abundance of each

368 segment in the purified supernatant. It is possible that the abundance of replication
369 competent / infectious RNA for each segment are similar, and that the increased
370 abundance of M and L RNA in the supernatant are representative of increased defective
371 RNA production for those segments. It is also possible that additional copies of M and L
372 are needed to efficiently initiate viral replication in a newly infected cell. In a previous
373 study by Bermudez-Mendez et al using the orthobunyavirus, Schmallenberg Virus
374 (SBV), the authors found relative segment abundance to be dependent on the cell line
375 infected [32]. Specifically, Vero cells infected with SBV were found to release different
376 abundances of the S, M, and L genomes, but infection of C6/36 mosquito cells resulted
377 in the release of more equivalent amounts of all three segments. Therefore, it is
378 possible that relative segment abundance may be context- and virus-dependent, and
379 warrants future study.

380 A further consideration is the possibility that purified supernatants contain viral
381 particles along with extracellular vesicles. Endothelial cells have been reported to
382 generate extracellular vesicles for communication with other cells and viral RNA has
383 been found within extracellular vesicles in other viral systems. Thus, the composition of
384 particles in the cellular supernatant may influence the measured abundance of each
385 segment and may be found to play a role in infection dynamics and pathogenesis for
386 hantaviruses in the future.

387 Contrary to our hypothesis, although SEOV RNA was more abundant in the rat
388 endothelial cells compared to human endothelial cells, a finding consistent with previous
389 literature, the temporal kinetics of RNA accumulation and release remained similar
390 between the two species [33]. The human and rat endothelial cells reach maximum

391 RNA accumulation and viral titer by 2dpi. In contrast, the Vero cells show consistent
392 increases throughout infection. These data suggest that SEOV may replicate differently
393 in endothelial cells versus epithelial cells. However, it is important to note that infection
394 of Vero cells, while epithelial, are not representative of what infection of reservoir or
395 non-reservoir epithelial cells, as Vero cells lack a type I IFN response. Therefore,
396 analysis in additional relevant epithelial cell types and additional strains of SEOV would
397 be of interest. The lack of a strong type I IFN response during SEOV infection of
398 RLMVEC and Vero cells suggests that these temporal differences are not driven solely
399 by innate immune responses, but rather may be cell type specific [7]. Additionally,
400 SEOV has been proposed to use the same receptors, αVβ3 integrins, on both Vero and
401 endothelial cells, indicating that receptor usage may not explain this difference [34].
402 Therefore, it is possible that the variance seen in replication kinetics between the
403 endothelial cells and the epithelial cells are due to the unique virus : host interactions
404 that occur within each cell type. As such, future work will focus on defining virus : host
405 interactions unique to reservoir and non-reservoir infections and their consequences for
406 SEOV replication.
407

408 ## Materials and Methods
409
410 ***In Vitro* Transcription of SEOV RNAs**

411 Full length SEOV S genomic RNA was *in vitro* transcribed from PCR templates using
412 the T7 MEGAscript kit (Ambion AM1334) according to manufacturer's instructions. Full
413 length M and L genomes were unable to be obtained with this method, so 500nt
414 segments spanning the primer and probe binding regions were PCR amplified using the

415 primers in table 1 (underlined portions indicate T7 promoter). These PCR templates
416 were then *in vitro* transcribed using the T7 MEGAshortscript kit (Ambion AM1354). For
417 full length antigenomic SEOV RNA, plasmids containing each of the positive sense RNA
418 segments with an upstream T7 promoter sequence were linearized with NheI and then
419 used as templates for *in vitro* transcription using the T7 MEGAscript kit according to
420 manufacturer's instructions.
421 To assess RNA integrity, RNA ladder (Thermo Scientific High Range RiboRuler
422 FERSM1821) or IVT RNA was mixed with RNA loading dye containing ethidium
423 bromide, heated to 80°C for 10 minutes, placed immediately on ice, and then run at 30V
424 on a 2% formaldehyde-agarose gel. RNA bands were visualized using a BioRad
425 ChemiDoc imaging system. Concentrations of the RNA transcripts were measured
426 using spectrophotometry and the molecules RNA/uL for each transcript was calculated
427 using the total molecular weight of each RNA segment.
428 Table 1. PCR Primers for Genomic IVT templates.

S For	gcccgggtagtagtagctcccta
S T7 Rev	taatacgactcactatagggctagctagtagtatctcccta
M 500nt For	ccacagctgcacttttgattac
M 500nt T7 Rev	taatacgactcactatagggatttctgctgcacttgctg
L 500nt For	ggttcttatttgtatcccagc
L 500nt T7 Rev	taatacgactcactatagggcctataccggctgttgaaag

429 *Underlined sequences indicate the T7 promoter
430 **cDNA Synthesis**

431 IVT RNA was mixed with 50uM dNTPs and either 1uM (S and M) or 0.1uM (L) cDNA
432 primer (Table 2, uppercase indicates tag sequence), heated at 95C for 5min, and then
433 immediately moved to ice. RT buffer (Maxima H-minus reverse transcription kit, Thermo
434 Scientific K1652) and RNAse inhibitor (Abmgood G138) were then added to the
435 reaction. The reaction was then moved to either 60C (M and L) or 65C (S) and Maxima
436 H-minus reverse transcriptase was added. Reactions were then moved to 65C for
437 30min, followed by 85C for 5min, then cooled to 4C. RNase H (NEB M0297L) was
438 added to each reaction and incubated at 37C for 20min. To measure cDNA synthesis
439 resulting from self-priming RNAs, cDNA synthesis was carried out in the absence of the
440 cDNA primer. For both the validation assays using host RNAs and to experimentally
441 measure intracellular viral RNA, 500ng cellular RNA were used as input. To measure
442 genomic RNA release, 25% of RNA extracted from pelleted supernatants was used as
443 input.
444 cDNA synthesis for total viral RNA SYBR qRT-PCR was done using a high capacity
445 cDNA reverse transcription kit (Applied Biosystems 4368814) following manufacturer's
446 instructions. For both the validation assays using host RNAs and to measure
447 intracellular viral RNA, 500ng cellular RNA were used as input. Validation assays using
448 mixed host and IVT RNAs used 150ng cellular RNA as input.
449 Table 2. cDNA Primers

S Genome	GCATGCTCGTGGACAGACTAaatcgtgactatatcagacaga
M Genome	CTGCGTGAGTATCCTACCGCagaaccgattcaaagccattctacg
L Genome	GCGCTACTGTGAGAGACGTAcaatctgcatgagcacatcc

450 *Capitalized sequences correspond to PCR tag

451 **qRT-PCR**

452 The ssqRT-PCR assay was performed using 300nM segment-specific qPCR primer,
453 300nM segment specific tag primer, 200nM Taqman probe, and PrimeTime Gene
454 Expression Master Mix (IDT 1055771; Table 3). Standard curves were generated using
455 cDNA made from IVT RNAs such that a range of 1x10^6 copies to 1 copy cDNA were
456 added to the ssqRT-PCR reaction. Thermocycling conditions for S: 95C for 3min, 40
457 cycles of 95C for 15sec and 70C for 1min. Thermocycling conditions for M and L: 95C
458 for 3min, 40 cycles of 95C for 15sec and 60C for 1min. For infections, copy number/ng
459 and copy number/mL was calculated using a standard curve from IVT genomic RNA.
460 SYBR qRT-PCR was performed using Applied Biosystems SYBR Green Universal
461 master mix (4309155) following manufacturer's guidelines. cDNA was diluted to within
462 range of the standard curve then mixed with 12.5nM segment specific forward and
463 reverse primers and 1x SYBR mix. Thermocycling conditions: 95C for 10min, 40 cycles
464 of 95C for 15sec and 60C for 1min. For infections, copy number/ng and copy
465 number/mL was calculated using a standard curve from IVT genomic RNA.

466 Table 3. qRT-PCR Primers and Probe

S Genome Tag	GCATGCTCGTGGACAGACTA
S Genome qPCR	cacctaattcagccatccctccg
S Genome Probe (Cy5)	tggctccatccctgcaagtgcacc
M Genome Tag	CTGCGTGAGTATCCTACCGC
M Genome qPCR	cttctctgaatcggtgggtggc
M Genome Probe (Tamra)	acccactgtgaaccgacagaaactgc
L Genome Tag	GCGCTACTGTGAGAGACGTA

L Genome qPCR	tcgctttgacgcatctcgt
L Genome Probe (Fam)	agggaattgatacagcacagccctca
S SYBR qPCR Forward	gcaaattcatggcggagtct
S SYBR qPCR Reverse	gttgcctgagggcttgaaat
M SYBR qPCR Forward	tgttcaaggagagtgcccat
M SYBR qPCR Reverse	gtgggtggcttgacaaactt
L SYBR qPCR Forward	ttgagggctgtgctgtatca
L SYBR qPCR Reverse	aaatccatcgctttgacgca

467

468 **Cell Culture and Virus Propagation**

469 Vero E6 cells (ATCC, CRL-1586) were cultured in Dulbecco's modified Eagle's medium
470 (DMEM) supplemented with 1% pen/strep, 1% nonessential amino acids, 10% heat
471 inactivated FBS, and 2.5% HEPES. Primary rat lung microvascular endothelial cells
472 (RLMVEC, VEC Technologies) were cultured in MCDB-131 base medium (Corning)
473 supplemented with VascuLife VEGF LifeFactors (Lifeline Cell Technology LS-1020) and
474 10% heat inactivated FBS. Human umbilical vein endothelial cells (HUVEC-C; ATCC,
475 CRL-1730) were cultured in VascuLife EnGS Endothelial medium (Lifeline Cell
476 Technology LM-0002) with VascuLife EnGS LifeFactors (Lifeline Cell Technology LS-
477 1019) and 10% heat inactivated FBS. All cells were cultured at 37C and 5% CO_2.
478 Endothelial cells were cultured on tissue culture treated plates coated with rat tail
479 collagen (VWR, 47747-218).

480 To propagate virus, Vero E6 cells were infected with Seoul virus (SEOV) strain SR11 for
481 12 days (MOI 0.01). Supernatant was then collected and clarified by centrifugation at
482 1000xg for 10min.

483 **Virus Infections**

484 RLMVEC, HUVEC, and Vero E6 cells were infected with SEOV at a cell-specific
485 multiplicity of infection (MOI) of 0.1 focus forming units / cell. Cell specific MOI was
486 determined previously [7]. After a 1hr adsorption period at 37C, the inoculum was
487 removed, and the cells were washed twice with 1x phosphate buffered saline (PBS) to
488 remove unbound virus. Each cell line was given its respective media and incubated at
489 37C and 5% CO_2. At the indicated times post infection, supernatant was collected and
490 clarified at 1000xg for 10min. An aliquot (25%, 500uL) of supernatant was kept for
491 measuring viral titer while the rest (75%, 1.5mL) was inactivated by applying UV
492 radiation at 104,000 uJ/cm^2 (FisherBrand UV crosslinker, 13-245-221). Virus from UV
493 inactivated supernatant was pelleted though a 30% w/v sucrose cushion in TNE buffer
494 (10mM Tris-HCl pH 7.5, 100mM NaCl, 1mM EDTA) for 2hrs at 30,000rpm. TRIzol
495 reagent was added to the pellets and total RNA was extracted via isolation following
496 manufacturer instructions. Cell monolayers were washed with 1x PBS and harvested in
497 TRIzol reagent (ThermoFisher Scientific, 15596026). Total RNA was extracted via
498 isolation following manufacturer's instructions.

499 **Focus Forming Unit Assay**

500 Standard virological focus forming unit (FFU) assays were used to determine the
501 infectious titer of all viral samples as previously described [11]. Briefly, Vero E6 cells
502 were inoculated with 5-fold or 10-fold serial dilutions of virus containing samples. After a

503 1hr adsorption period, cells were overlaid with 2% methylcellulose supplemented with
504 2x DMEM, 2% FBS, 1% pen/strep, and 1% HEPES. At 7dpi, cells were fixed with 95%
505 EtOH : 5% acetic acid and probed with primary anti-SEOV N (custom, Genscript) and
506 HRP-conjugated goat anti-mouse antibodies (JacksonImmunoresearch, 115-035-003).
507 Foci were visualized using Vector VIP peroxidase substrate kit (Vector Laboratories,
508 SK-4600).
509

510 **Figures**

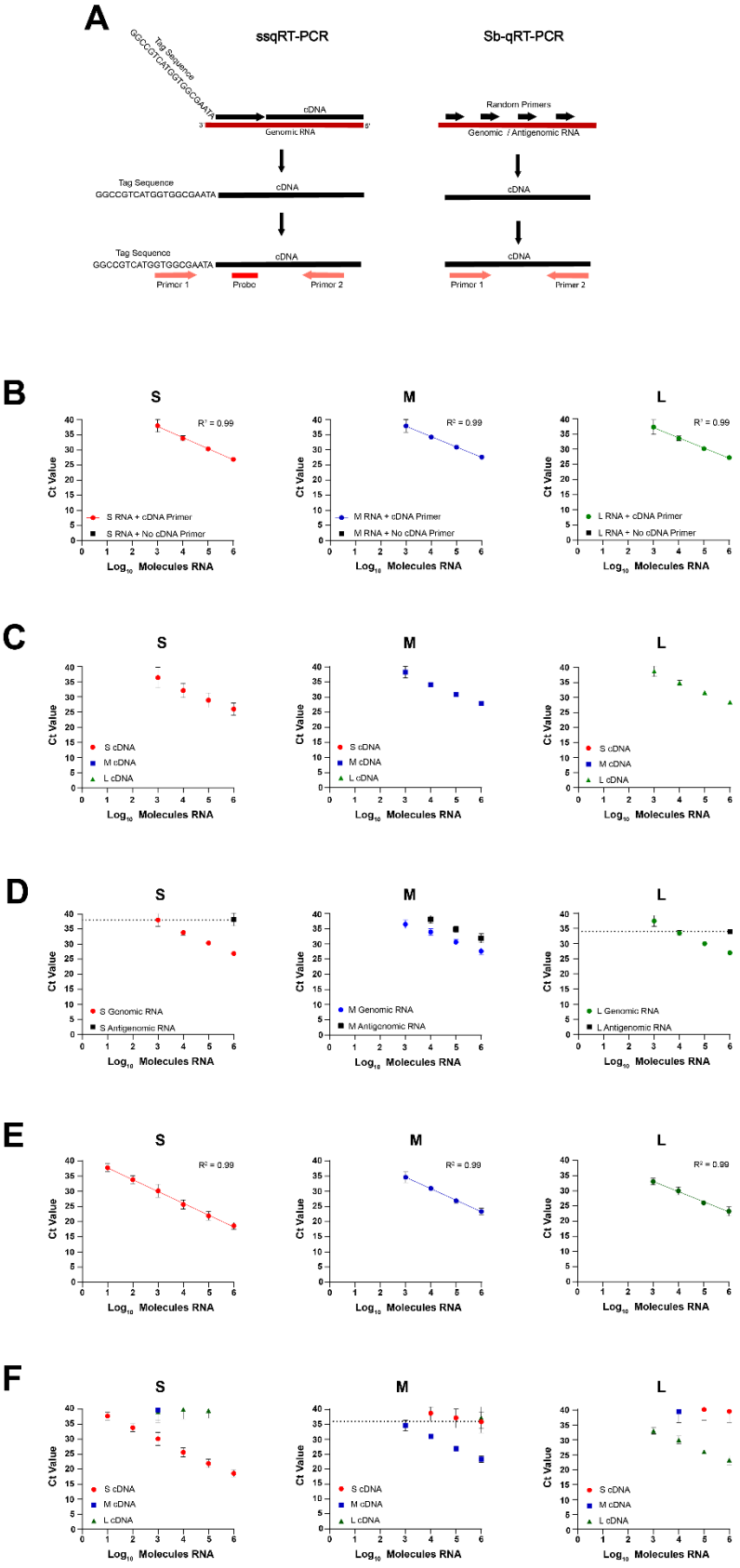

511

512 **Figure 1. Validation of the ssqRT-PCR and Sb-qRT-PCR using *in vitro* transcribed**
513 **RNAs.** (A) Schematic of the cDNA synthesis and qRT-PCR strategies for the ssqRT-
514 PCR and Sb-qRT-PCR assays. Standard curves using serial 10-fold dilutions of either
515 S, M, or L negative-sense IVT RNAs (red circles = S, blue squares = M, green triangles
516 = L) in the ssqRT-PCR assays (B-D) or Sb-qRT-PCR assays (E,F). (B, E) Assay
517 sensitivity was determined by using serial dilutions of S, M, or L IVT RNA with the
518 paired primers/probe for each assay, and dotted lines represent C_t cutoff for reliable
519 template quantification using the respective assay. (C, F) Segment specificity was
520 determined by using S, M, or L IVT RNA individually against the each segment's
521 primers/probe (primer/probe used is indicated in the graph titles). Data shown
522 represent the mean of ≥3 independent experiments ±SD.
523
524

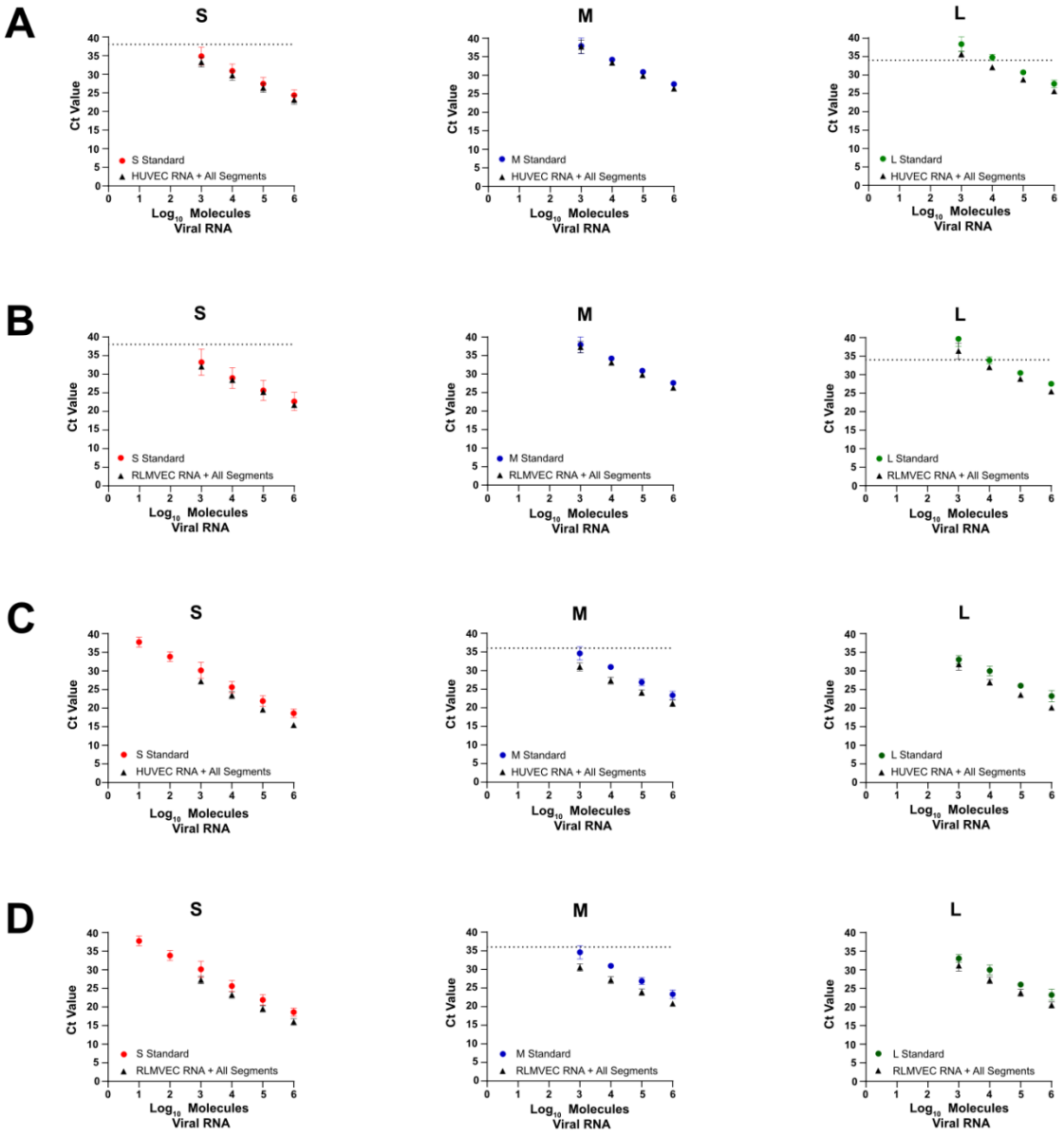

525

526 **Figure 2. ssqRT-PCR and Sb-qPCR assays do not detect RNAs from uninfected**

527 **host cells.** To validate that neither the ssqRT-PCR assay (A, B) nor the Sb-qRT-PCR

528 assay (C,D) detected host cellular RNAs, standard curves were made using serial

529 dilutions of S, M, or L negative-sense IVT RNA (circles) or a mixture of 10^6 copies per

530 strand of S, M, and L genomic and antigenomic IVT RNAs plus 150ng of either

531 uninfected HUVEC (A,C) or uninfected RLMVEC (B, D) RNA (triangles). The IVT RNA

532 alone or mixture of IVT RNAs and uninfected cellular RNA was then used as input for
533 either the ssqRT-PCR assay (A,B) or SB-qRT-PCR (C,D) assay using the
534 primers/probe indicated in the graph title. Data shown represent the mean of ≥3
535 independent experiments ±SD.
536

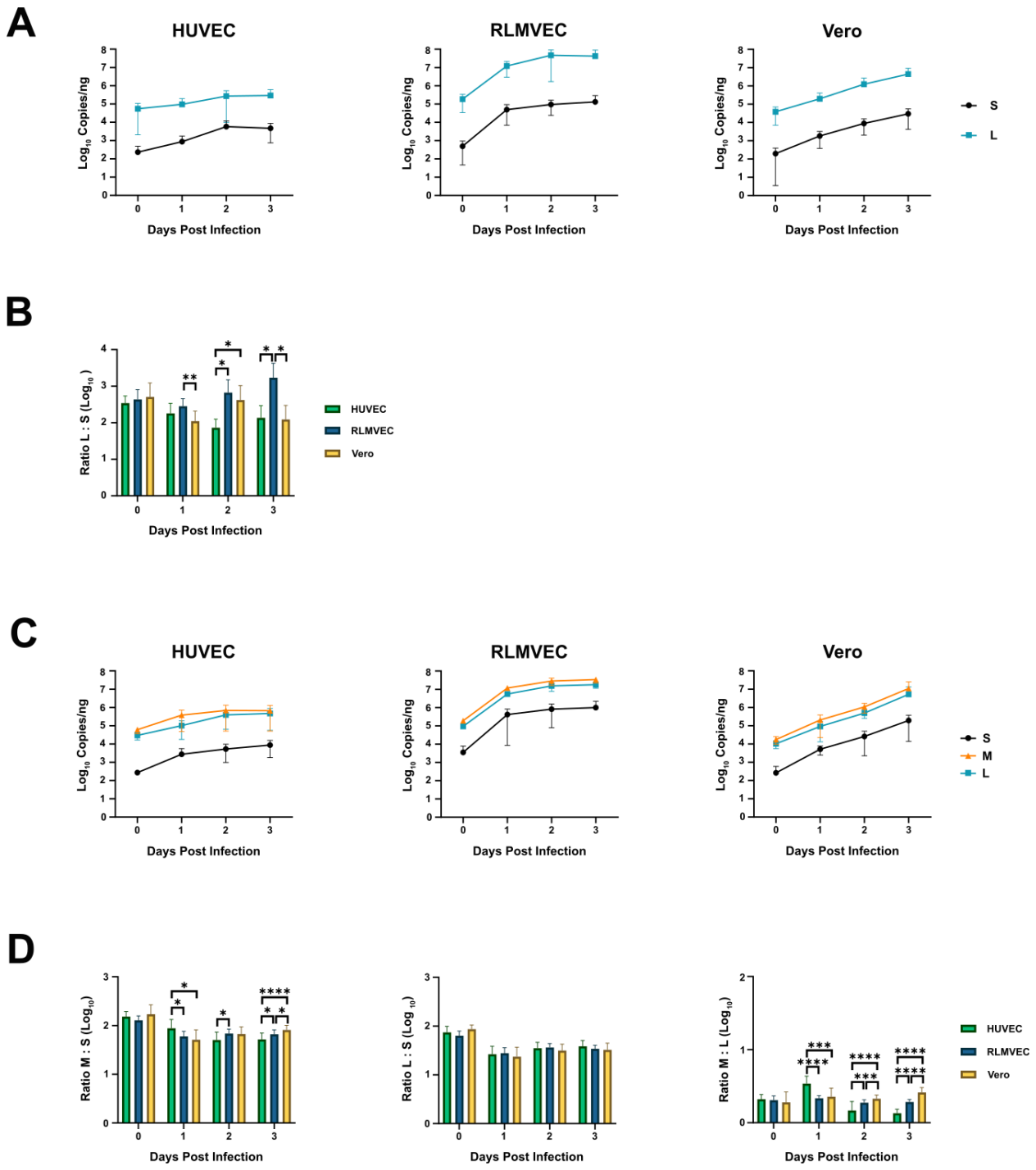

537

538 **Figure 3. Quantification of viral RNA in SEOV-infected reservoir and non-reservoir**

539 **cells.** HUVEC, RLMVEC, and Vero cells were infected with SEOV at an MOI of 0.1

540 FFU/cell. Cells were harvested and RNA extracted at the indicated days post infection.

541 (A) S and L genomic RNA accumulation was measured using ssqRT-PCR for each cell

542 type. (B) The ratio of L RNA copies to S RNA copies was then calculated for each time
543 point. (C) Combined positive and negative sense viral RNA accumulation was
544 measured using Sb-qRT-PCR for all three segments. (D) The ratios of M RNA copies to
545 S RNA copies, L RNA copies to S RNA copies, and M RNA copies to L RNA copies
546 were then calculated for each time point. Data shown represent the mean of ≥3
547 independent experiments ±SD. Statistical significance determined by Student's t test. *,
548 $p<0.05$; **, $p<0.01$; ***, $p<0.001$, ****, $p<0.0001$.
549
550
551
552
553

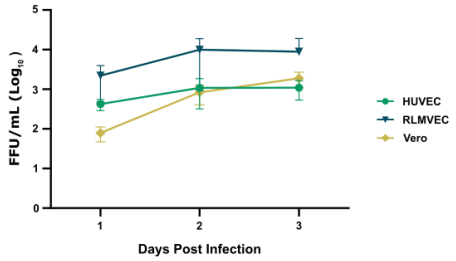

B

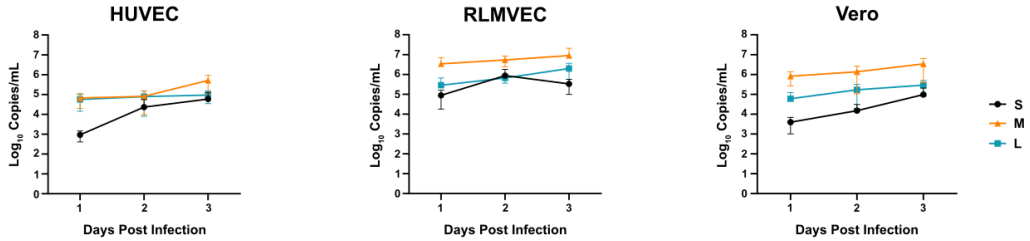

C

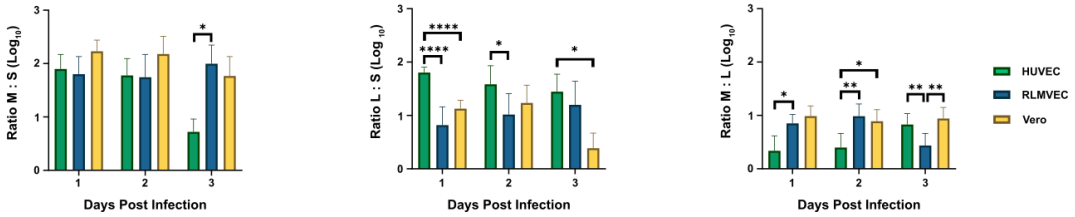

Figure 4. Quantification of infectious virus and RNA genome release from SEOV-infected cells. HUVEC, RLMVEC, and Vero cells were infected with SEOV at an MOI of 0.1 FFU/cell. (A, B) Supernatants were collected at the indicated times post infection and used for either measuring viral titer via FFU assay (A) or RNA extracted to measure genomic RNA via the ssqRT-PCR assay (B). (C) Ratios of M RNA copies to S RNA copies, L RNA copies to S RNA copies, and M RNA copies to L RNA copies were calculated for each time point. Data shown represent the mean of ≥3 independent experiments ±SD. Statistical significance determined by Student's t test. *, $p<0.05$; **, $p<0.01$; ***, $p<0.001$, ****, $p<0.0001$.

565

566 ## Author Contributions

567 Conceptualization: A.T.L and A.M.K; investigation: A.T.L., S.D.K., and A.M.K.; writing
568 original draft: A.T.L. and A.M.K.; review and editing: A.T.L., S.D.K., and A.M.K.;
569 supervision: A.M.K.

570

571 ## Conflicts of Interest

572 The authors declare that there are no conflicts of interest.

573

574 ## Funding Information

575 This work was supported by the National Institutes of Health NIAID grant
576 1R01AI171289-01 granted to AMK. ATL and SDK were supported by fellowships by the
577 National Institutes of Health NIGMS T32AI007538. The funders had no role in study
578 design, data collection and analysis, decision to publish, or preparation of the
579 manuscript.

580

581 ## Acknowledgements

582 We would like to acknowledge Dr. Dave Peabody for the use of space and helpful
583 feedback.

584

585 ## References

586 1. Schountz, T. and J. Prescott, *Hantavirus immunology of rodent reservoirs:*
587 *current status and future directions.* Viruses, 2014. **6**(3): p. 1317-35.
588 2. Maas, M., et al., *Seoul Virus Tropism and Pathology in Naturally Infected Feeder*
589 *Rats.* Viruses, 2019. **11**(6).
590 3. Kell, A.M., *Innate Immunity to Orthohantaviruses: Could Divergent Immune*
591 *Interactions Explain Host-specific Disease Outcomes?* J Mol Biol, 2022. **434**(6):
592 p. 167230.
593 4. Jonsson, C.B., L.T. Figueiredo, and O. Vapalahti, *A global perspective on*
594 *hantavirus ecology, epidemiology, and disease.* Clin Microbiol Rev, 2010. **23**(2):
595 p. 412-41.
596 5. Zhang, Y.Z., et al., *Hantavirus infections in humans and animals, China.* Emerg
597 Infect Dis, 2010. **16**(8): p. 1195-203.
598 6. Martinez, V.P., et al., *"Super-Spreaders" and Person-to-Person Transmission of*
599 *Andes Virus in Argentina.* N Engl J Med, 2020. **383**(23): p. 2230-2241.
600 7. Klimaj, S.D., et al., *Seoul orthohantavirus evades innate immune activation by*
601 *reservoir endothelial cells.* PLoS Pathog, 2024. **20**(11): p. e1012728.
602 8. Valbuena, G. and D.H. Walker, *The endothelium as a target for infections.* Annu
603 Rev Pathol, 2006. **1**: p. 171-98.
604 9. Ermonval, M., F. Baychelier, and N. Tordo, *What Do We Know about How*
605 *Hantaviruses Interact with Their Different Hosts?* Viruses, 2016. **8**(8).
606 10. Mackow, E.R., et al., *Hantavirus interferon regulation and virulence determinants.*
607 Virus Res, 2014. **187**: p. 65-71.

608 11. Kell, A.M., et al., *RIG-I-like receptor activation drives type I IFN and antiviral*
609 *signaling to limit Hantaan orthohantavirus replication.* PLoS Pathog, 2020. **16**(4):
610 p. e1008483.
611 12. LaPointe, A., M. Gale, Jr., and A.M. Kell, *Orthohantavirus Replication in the*
612 *Context of Innate Immunity.* Viruses, 2023. **15**(5).
613 13. Easterbrook, J.D. and S.L. Klein, *Seoul virus enhances regulatory and reduces*
614 *proinflammatory responses in male Norway rats.* J Med Virol, 2008. **80**(7): p.
615 1308-18.
616 14. Strandin, T., et al., *Orthohantavirus Isolated in Reservoir Host Cells Displays*
617 *Minimal Genetic Changes and Retains Wild-Type Infection Properties.* Viruses,
618 2020. **12**(4).
619 15. Li, W. and S.L. Klein, *Seoul virus-infected rat lung endothelial cells and alveolar*
620 *macrophages differ in their ability to support virus replication and induce*
621 *regulatory T cell phenotypes.* J Virol, 2012. **86**(21): p. 11845-55.
622 16. Garcin, D., et al., *The 5' ends of Hantaan virus (Bunyaviridae) RNAs suggest a*
623 *prime-and-realign mechanism for the initiation of RNA synthesis.* J Virol, 1995.
624 **69**(9): p. 5754-62.
625 17. Jeeva, S., et al., *Hantavirus RdRp Requires a Host Cell Factor for Cap*
626 *Snatching.* J Virol, 2019. **93**(5).
627 18. Hutchinson, K.L., C.J. Peters, and S.T. Nichol, *Sin Nombre virus mRNA*
628 *synthesis.* Virology, 1996. **224**(1): p. 139-49.

629 19. Tercero, B., et al., *A strand-specific real-time quantitative RT-PCR assay for*
630 *distinguishing the genomic and antigenomic RNAs of Rift Valley fever*
631 *phlebovirus.* J Virol Methods, 2019. **272**: p. 113701.
632 20. Barnard, T.R., A.B. Wang, and S.M. Sagan, *A highly sensitive strand-specific*
633 *multiplex RT-qPCR assay for quantitation of Zika virus replication.* J Virol
634 Methods, 2022. **307**: p. 114556.
635 21. Tercero, B., et al., *Mechanistic insight into the efficient packaging of antigenomic*
636 *S RNA into Rift Valley fever virus particles.* Front Cell Infect Microbiol, 2023. **13**:
637 p. 1132757.
638 22. Wigren Bystrom, J., et al., *Quantification and kinetics of viral RNA transcripts*
639 *produced in Orthohantavirus infected cells.* Virol J, 2018. **15**(1): p. 18.
640 23. Thompson, K.A. and J. Yin, *Population dynamics of an RNA virus and its*
641 *defective interfering particles in passage cultures.* Virol J, 2010. **7**: p. 257.
642 24. Brown, C.M. and K.D. Bidle, *Attenuation of virus production at high multiplicities*
643 *of infection in Aureococcus anophagefferens.* Virology, 2014. **466-467**: p. 71-81.
644 25. Brennan, J.W. and Y. Sun, Defective viral genomes: advances in understanding
645 their generation, function, and impact on infection outcomes. mBio, 2024. 15(5):
646 p. e0069224.
647 26. Vera-Otarola, J., et al., *The Andes hantavirus NSs protein is expressed from the*
648 *viral small mRNA by a leaky scanning mechanism.* J Virol, 2012. **86**(4): p. 2176-
649 87.

650 27. Jaaskelainen, K.M., et al., *Tula and Puumala hantavirus NSs ORFs are*
651 *functional and the products inhibit activation of the interferon-beta promoter.* J
652 Med Virol, 2007. **79**(10): p. 1527-36.
653 28. Binder, F., et al., *Inhibition of interferon I induction by non-structural protein NSs*
654 *of Puumala virus and other vole-associated orthohantaviruses: phenotypic*
655 *plasticity of the protein and potential functional domains.* Arch Virol, 2021.
656 **166**(11): p. 2999-3012.
657 29. Plyusnin, A., *Genetics of hantaviruses: implications to taxonomy.* Arch Virol,
658 2002. **147**(4): p. 665-82.
659 30. Rezelj, V.V., et al., *M Segment-Based Minigenomes and Virus-Like Particle*
660 *Assays as an Approach To Assess the Potential of Tick-Borne Phlebovirus*
661 *Genome Reassortment.* J Virol, 2019. **93**(6).
662 31. Shrivastava-Ranjan, P., et al., Development of a novel minigenome and
663 recombinant VSV expressing Seoul hantavirus glycoprotein-based assays to
664 identify anti-hantavirus therapeutics. Antiviral Res, 2023. 214: p. 105619.
665 32. Bermudez-Mendez, E., et al., Visualizing the ribonucleoprotein content of single
666 bunyavirus virions reveals more efficient genome packaging in the arthropod
667 host. Commun Biol, 2021. 4(1): p. 345.
668 33. Noack, D., et al., Species-specific responses during Seoul orthohantavirus
669 infection in human and rat lung microvascular endothelial cells. PLoS Negl Trop
670 Dis, 2024. 18(3): p. e0012074.

671 34. Gavrilovskaya, I.N., et al., *Cellular entry of hantaviruses which cause*
672 *hemorrhagic fever with renal syndrome is mediated by beta3 integrins.* J Virol,
673 1999. **73**(5): p. 3951-9.
674
675

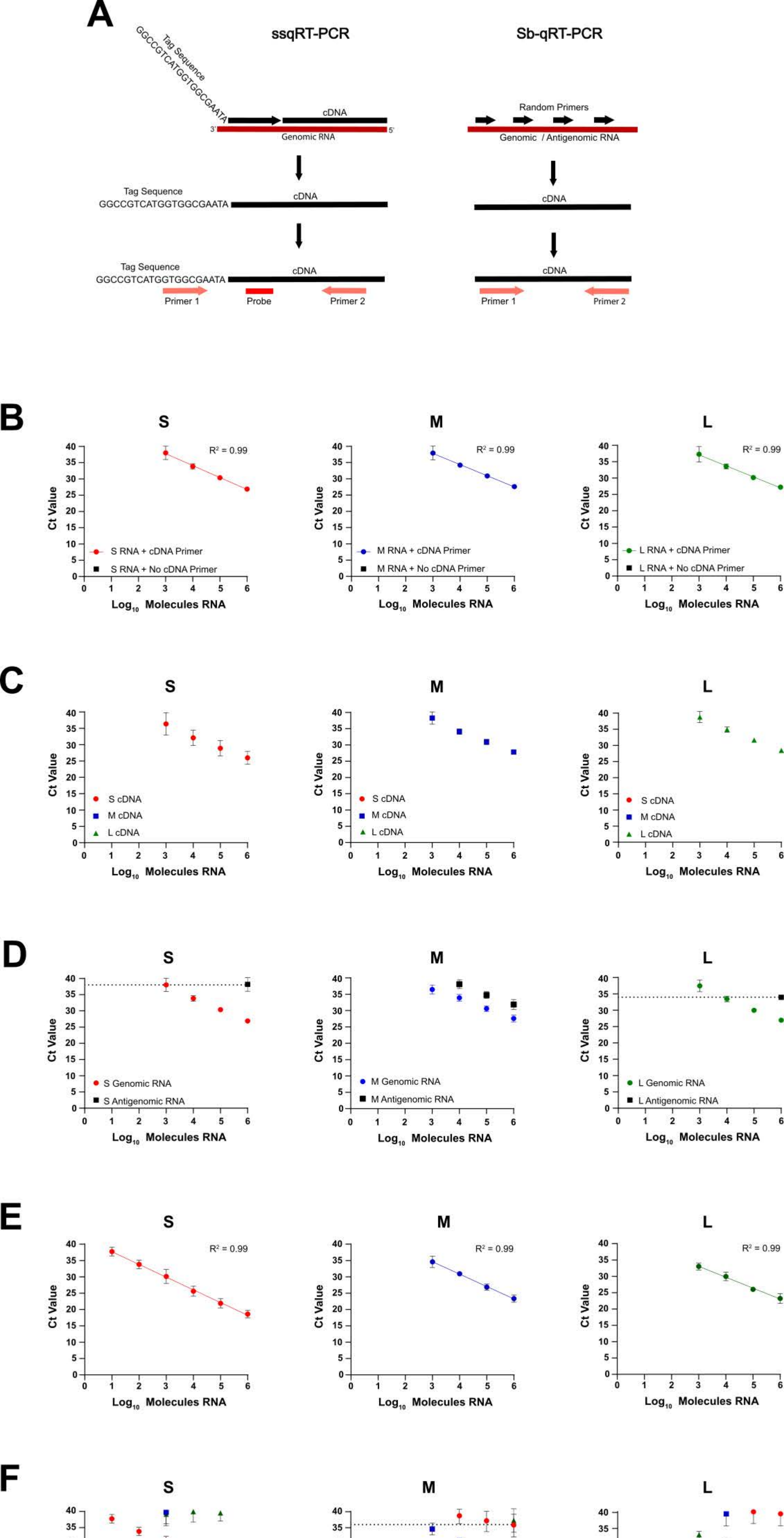
A
ssqRT-PCR
Sb-qRT-PCR
Tag Sequence
GGCCGTCATGGTGGCGAATA
cDNA
3'
5'
Genomic RNA
Random Primers
Genomic / Antigenomic RNA
Tag Sequence
GGCCGTCATGGTGGCGAATA
cDNA
Tag Sequence
GGCCGTCATGGTGGCGAATA
cDNA
Primer 1
Probe
Primer 2
cDNA
Primer 1
Primer 2
B
S
M
L
R² = 0.99
Ct Value
S RNA + cDNA Primer
S RNA + No cDNA Primer
M RNA + cDNA Primer
M RNA + No cDNA Primer
L RNA + cDNA Primer
L RNA + No cDNA Primer
Log10 Molecules RNA
C
S cDNA
M cDNA
L cDNA
D
S Genomic RNA
S Antigenomic RNA
M Genomic RNA
M Antigenomic RNA
L Genomic RNA
L Antigenomic RNA
E
F

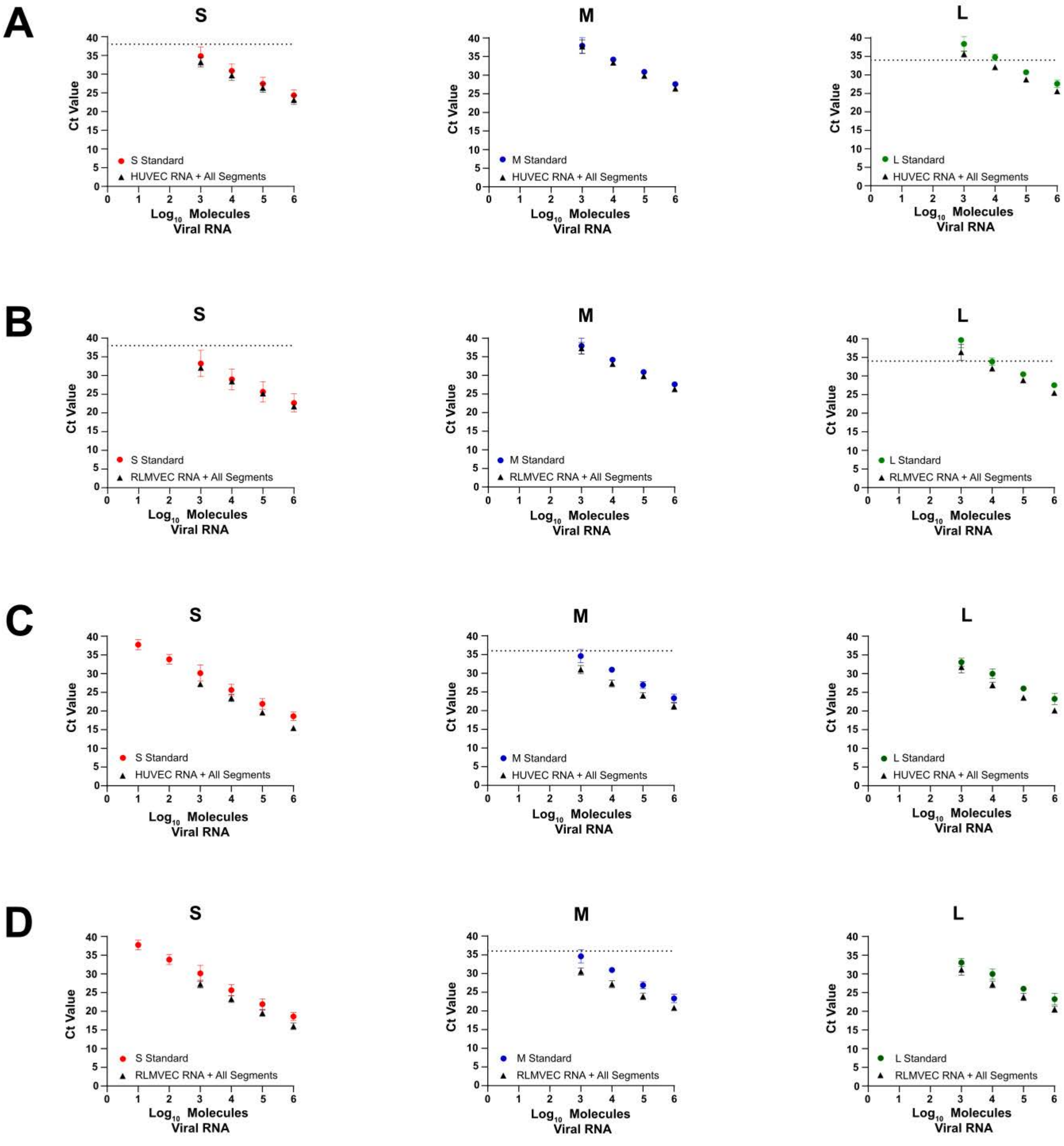
A
S
M
L
B
S
M
L
C
S
M
L
D
S
M
L
Ct Value
Log10 Molecules Viral RNA
S Standard
M Standard
L Standard
HUVEC RNA + All Segments
RLMVEC RNA + All Segments

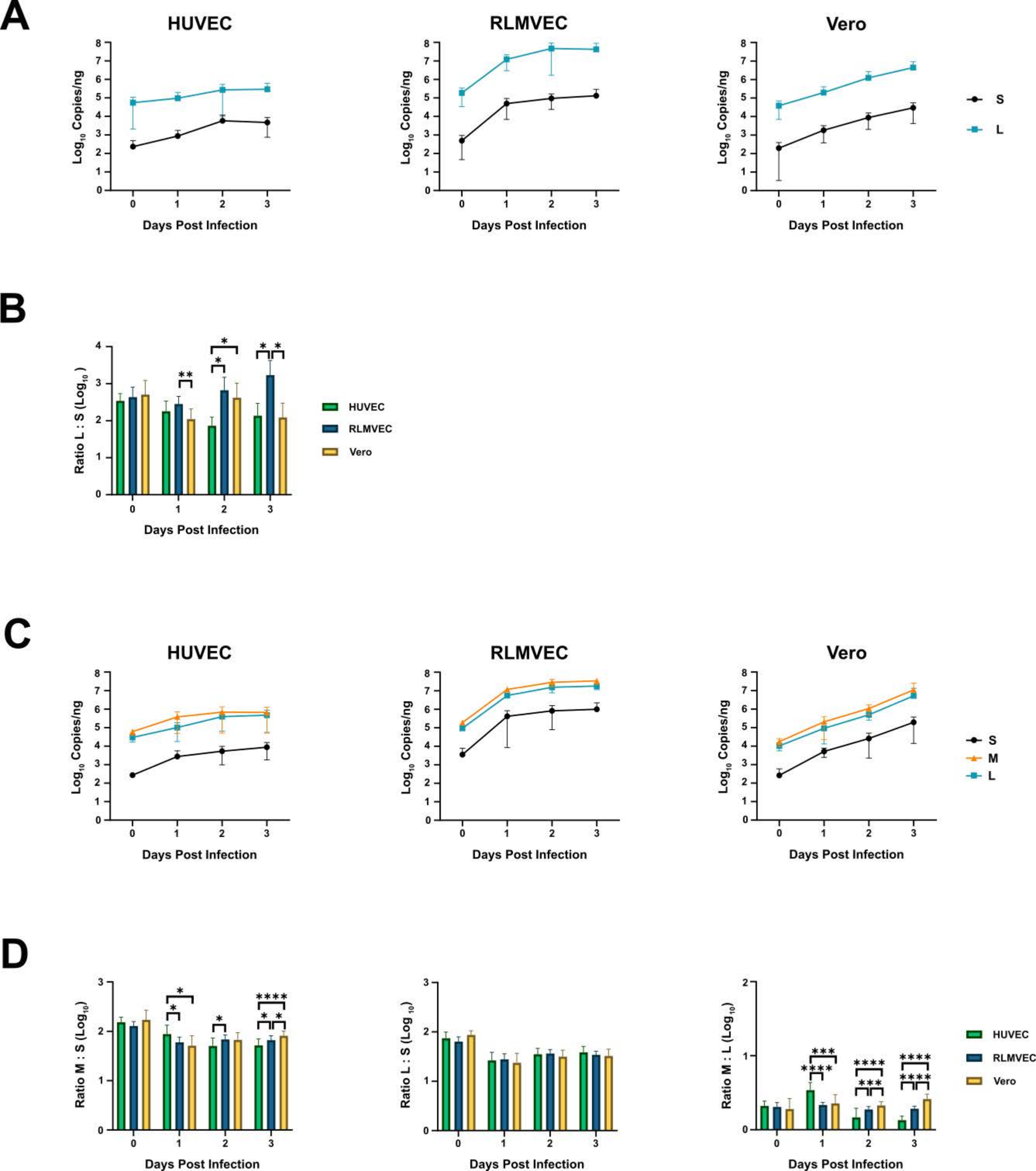
A
HUVEC
RLMVEC
Vero
Log10 Copies/ng
Days Post Infection
S
L
B
Ratio L : S (Log10)
Days Post Infection
HUVEC
RLMVEC
Vero
C
HUVEC
RLMVEC
Vero
Log10 Copies/ng
Days Post Infection
S
M
L
D
Ratio M : S (Log10)
Ratio L : S (Log 10)
Ratio M : L (Log10)
Days Post Infection
HUVEC
RLMVEC
Vero

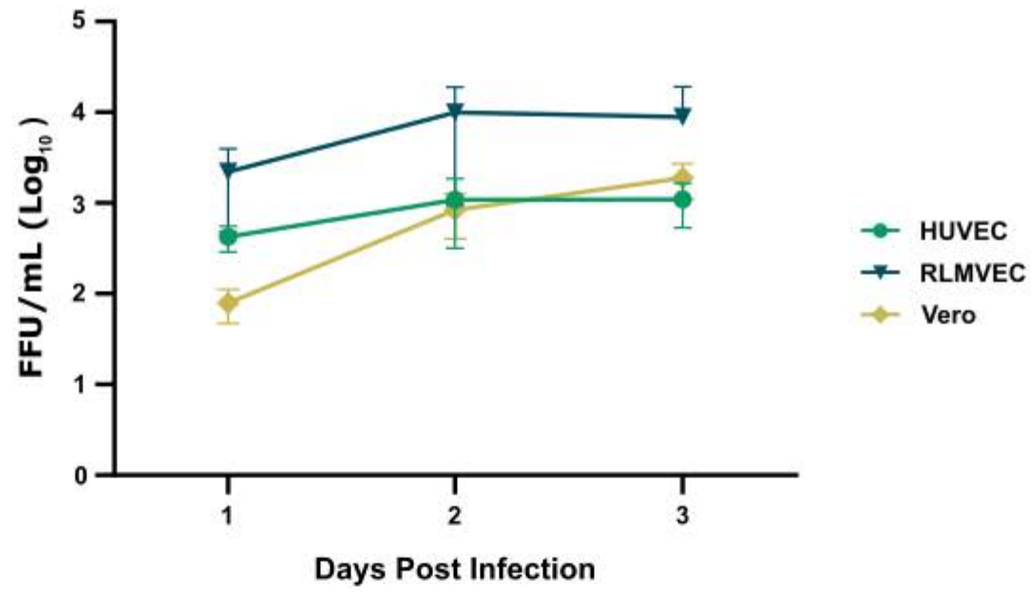
FFU/mL (Log10)
Days Post Infection
HUVEC
RLMVEC
Vero

B

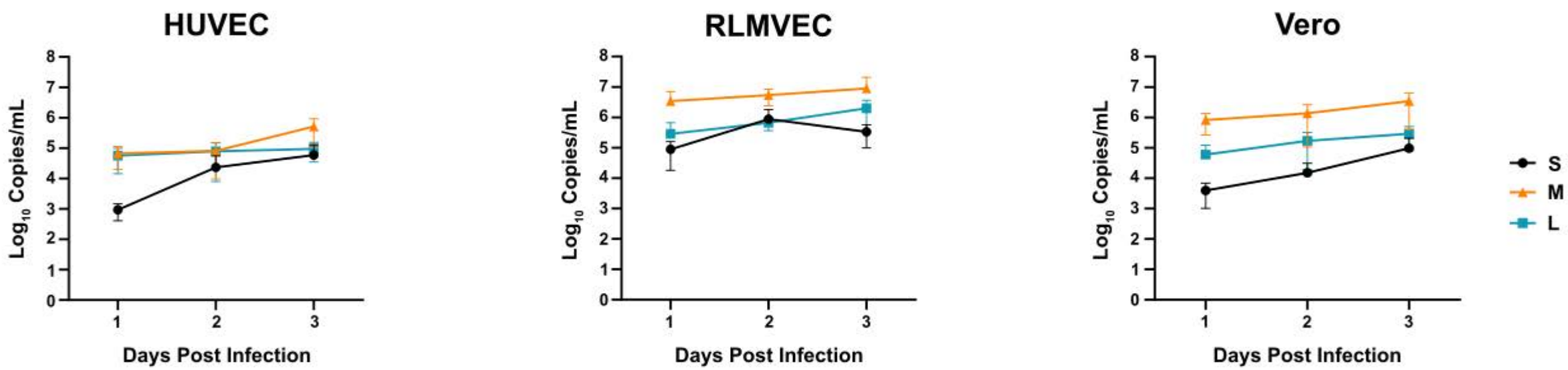
HUVEC
RLMVEC
Vero
Log10 Copies/mL
Days Post Infection
S
M
L

C

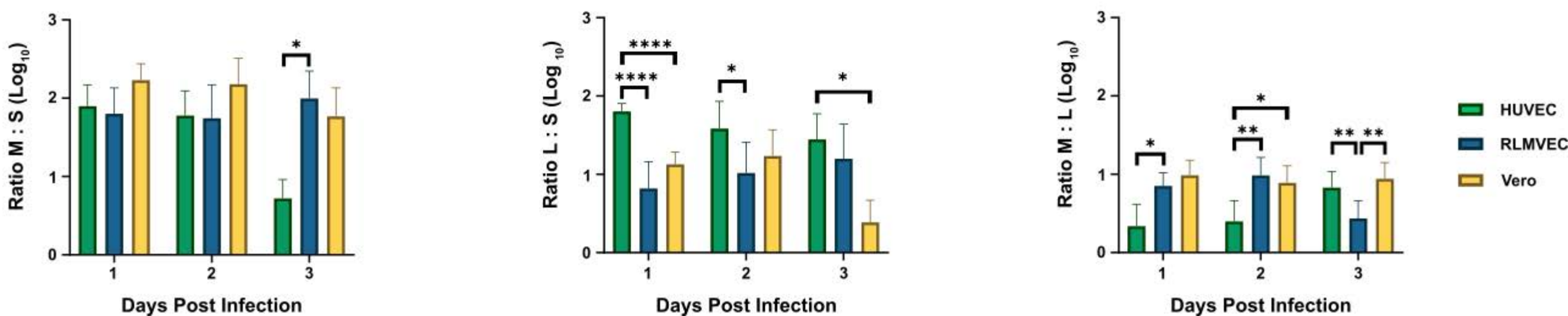
Ratio M : S (Log10)
Ratio L : S (Log 10)
Ratio M : L (Log10)
Days Post Infection
HUVEC
RLMVEC
Vero

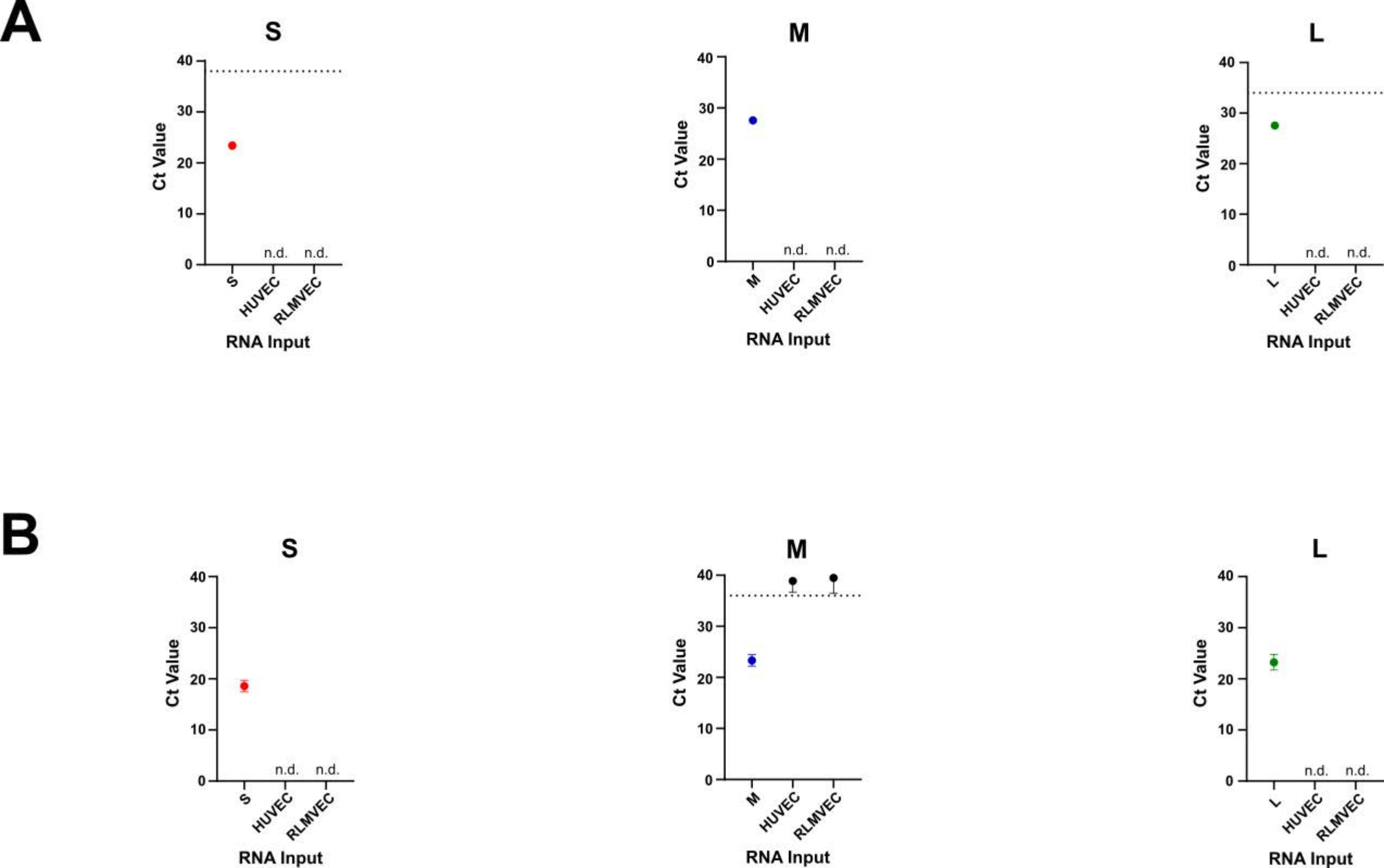
A
S
M
L
Ct Value
40
30
20
10
0
n.d.
n.d.
S
M
L
HUVEC
RLMVEC
RNA Input
B